# Precipitate Evolution and Creep Behavior of a W-Free Co-based Superalloy

QINYUAN LIU, JAMES COAKLEY, DAVID N. SEIDMAN, and DAVID C. DUNAND

The morphological and temporal evolution of $\gamma'$ (L1$_2$)-precipitates is studied in a polycrystalline Co-based superalloy (Co-30Ni-9.9Al-5.1Mo-1.9Nb at. pct) free of tungsten, aged at 1173 K (900 °C). Over a 1000 hours heat-treatment, the $\gamma'$ morphology evolves due to precipitate coalescence. The particles grow in size and the volume fraction decreases, while there is no significant change in the microhardness value. Compressional creep tests at 1123 K (850 °C) on a specimen aged at 1173 K (900 °C) demonstrate that the creep resistance is comparable to the original, W-containing, higher-density Co-based superalloy (Co-9Al-9.8W at. pct). This represents the first creep study of the Co-Al-Mo-Nb-based superalloy system. The W-free alloy exhibits directional coarsening of the $\gamma'$ precipitates in the direction perpendicular to the applied compressive stress, which indicates a positive misfit. This is consistent with neutron diffraction results.

## I. INTRODUCTION

N$_I$-BASED superalloys are utilized for turbine disks, blades, and jet engines owing to their high oxidation and corrosion resistance, and their excellent strength and creep behavior at ambient and elevated temperatures.[1,2] Ni-based superalloys are strengthened by coherent (L1$_2$) precipitates ($\gamma'$) with a base stoichiometry of Ni$_3$Al in a (fcc) Ni-rich matrix ($\gamma$).[3,4] Challenges remain, however, in both high-temperature strength[5] and hot-corrosion resistance[6,7] for Ni-based superalloys, indicating a need for new high-temperature alloys. In 2006, the $\gamma'$-Co$_3$(Al,W) phase, with a solvus temperature up to 1273 K (1000 °C), was reported in a new Co-based superalloy with the base composition Co-9.2Al-9W at. pct,[8] analogous to the $\gamma'$-Ni$_3$(Al,Ti) of Ni-based superalloys. Subsequent studies examined additions of Ti and Ta, which increase the solvus temperature and volume fraction of $\gamma'$.[9] Ductility is also enhanced in polycrystalline material with boron additions that strengthen the grain boundaries and suppresses intergranular fracture.[10] Creep resistance of Co-based alloys is increased with the addition of e.g., Cr, Mo, Ti, and Ta.[11–13] Furthermore, additions of

Ta,[14] Si[15], and Cr[16] increase oxidation resistance. The addition, however, of large quantities of W in these Co-based superalloys results in drawbacks. First, the low diffusivity of W[17] makes it difficult to homogenize the alloy. Second, the strength-to-weight ratio, which is essential for turbine blades, is lower due to the high density of W (yielding densities $> 9.3 \, \mathrm{gcm^{-3}}$). Finally, the presence of W results in deleterious precipitates, such as DO$_{19}$ (Co$_3$W).[18] In 2015, a new class of W-free Co-based superalloys was described[19,20] with a base composition Co-10Al-5Mo-2Nb at. pct. The microstructure of this alloy is analogous to Co-Al-W alloys with cuboidal $\gamma'$ [Co$_3$(Al, Mo, Nb)] precipitates coherently distributed in a $\gamma$-fcc Co-based matrix. With additions of Ni up to 30 at. pct, the solvus temperature is increased from 1159 K (886 °C) to 1263 K (990 °C), and the $\gamma'$ volume fraction is increased from 54 to 76 pct.[20] The density of the W-free alloys is decreased to 8.4gcm$^{-3}$ when compared to 9.2gcm$^{-3}$ for Co-7Al-7W at. pct.[20] The specific strength is also substantially improved. The specific strength reported for Co-30Ni-10Al-5Mo-2Nb is 96MPa/(gcm$^{-3}$) as compared to 79MPa/(gcm$^{-3}$) for Co-9Al-9.8W at. pct at room temperature.[20]

Much effort has been made in recent years to increase the $\gamma'$ solvus temperature of the Co-based superalloys,[9,21–24] while creep studies have primarily focused on the dislocation deformation mechanisms under tensile load, for example.[13,25,26] Rafting, also termed stress coarsening, occurs in superalloys during creep, and the orientation of the rafts (aligned coalesced $\gamma'$ particles), is dependent on the loading conditions (i.e., tensile vs compressive stress) and the lattice parameter misfit of the alloy $\delta = 2[a_{\gamma'} - a_{\gamma}]/[a_{\gamma'} + a_{\gamma}]$, where $a$ is the lattice parameter.[27] Co-based alloys developed thus far have all been of positive sign, and the rafts align parallel to the loading direction during tensile creep,[11] and are expected to align perpendicular to a compressive loading

QINYUAN LIU, Ph.D. Student, and DAVID C. DUNAND, Professor, are with the Department of Materials Science and Engineering, Northwestern University, Evanston, IL 60208-3108. JAMES COAKLEY, Research Fellow, is with the Department of Materials Science and Engineering, Northwestern University, and also with the Department of Materials Science and Metallurgy, University of Cambridge, Cambridge CB3 0FS, UK. Contact e-mail: james.coakley@northwestern.edu DAVID N. SEIDMAN, Professor, is with the Department of Materials Science and Engineering, Northwestern University, and also with the Northwestern University Center for Atom-Probe Tomography (NUCAPT), 2220 Campus Drive, Evanston, IL, 60208.

direction.[28] To the author's knowledge, the rafting orientations of Co-based superalloys have not been illustrated experimentally under compressive strain. In comparison, the lattice parameter misfit value of the Ni-based superalloys is typically negative, determined by X-ray/neutron diffraction techniques (e.g., References 29,30), resulting in the alignment of the $\gamma'$ particles in the opposite directions to those observed in Co-based superalloys.[31] At this point, it remains unclear which orientation is favorable to optimize mechanical properties of a superalloy.

The present study reports on the microstructural evolution of the Co-30Ni-10Al-5Mo-2Nb superalloy, and relates the microstructure to microhardness, creep, and lattice parameter misfit.

## II. EXPERIMENTAL PROCEDURES

The Co-30Ni-9.9Al-5.1Mo-1.9Nb at. pct alloy was arc melted under argon. The ingots were flipped and re-melted 8-10 times to ensure complete melting and homogenization of constituent elements. Samples were cut with a diamond saw from the as-cast ingots and vacuum-encapsulated in quartz tubes. Solutionizing of the sealed samples was performed at 1573 K (1300 °C) for 20 hours followed by quenching into cold water, aging at 1173 K (900 °C) for different times, and again water quenching. The $\gamma - \gamma'$ microstructure was imaged with a Hitachi SU8030 cold-field emission scanning electron microscope operated at 3 kV with a 3–5 mm working distance. SEM images of different areas of each aged sample were recorded after etching for ~2 seconds with a solution of 2.5 pct phosphoric acid in water by volume at 2.5 Vdc. The average room-temperature hardness was determined from 10 independent micro-hardness measurements using a Vickers indenter with a 9.8 N load.

Two cylindrical creep specimens (8.1 mm height and 4.0 mm diam.) were fabricated by electro-discharge machining from the ingot after aging at 1173 K (900 °C) for 200 hours. Multi-stress compressive creep tests were performed in air using a dead-load creep frame by placing the samples between two SiC platens lubricated with boron nitride. The tests were performed at 1123 K (850 °C) as measured by a thermocouple placed within 1 cm of the sample. The first sample was loaded at 150 MPa and held over a sufficiently long period of time to establish the minimum strain rate. Once the strain rate was established, the stress was increased to 185 MPa and held at this stress to establish the next minimum strain rate. This process was repeated two more times to a final stress of 236 MPa. The same methodology was applied to the second sample, with minimum strain rates measured at seven stress holds ranging from 115 to 305 MPa. Displacement was measured by a linear variable displacement transducer (LVDT) connected to the compression heads with a resolution of 2.5 $\mu$m. Strain rates were determined from slopes of the plots of strain against time.

A 6 mm × 7 mm surface area of a 900 °C/200 hours aged specimen (the same initial heat-treatment as the creep specimens) was chemically etched at room temperature with Carapellas reagent, swabbing for 3 to 4 seconds,[32] to inspect grain size by optical microscopy.

VULCAN, the time-of-flight Engineering Materials Diffractometer at the Spallation Neutron Source (SNS) in Oak Ridge National Laboratory, was used to measure the lattice parameter misfit at room temperature of the alloy aged at 1173 K (900 °C) for 200 hours. A $3 \times 5$ mm$^2$ cross section with 3-mm-thick tetragonal specimen was placed at 45 deg to the incident neutron beam, and diffracted neutrons were collected by two detector banks located at ±90 deg to the incident beam. The specimen was measured for 25 minutes using a beam power of 850 kW in the high-intensity mode with a chopper speed of 20 Hz. Neutron data reduction and initial analyses were conducted using the program VDRIVE.[33]

## III. RESULTS AND DISCUSSION

### A. Thermally Induced Precipitate Evolution

Figures 1(a) through (f) show SEM image cross-sectional views of the $\gamma/\gamma'$ microstructure as it evolves temporally at 1173 K (900 °C), after a solution treatment of a Co-30Ni-9.9Al-5.1Mo-1.9Nb at. pct alloy. This alloy exhibits uniform $\gamma'$-precipitates, with no other phase (e.g., DO$_{19}$) observed. Very fine $\gamma'$-precipitates, most probably associated with the cooling process, are present in the homogenized specimen, Figure 1(a). The $\gamma'$-precipitates in the specimen aged for 50 hours appear isolated, faceted, and cuboidal in morphology in the $\gamma$-matrix. The precipitates aged for 100 hours coalesce, and after 200 hours the $\gamma'$-precipitates become significantly directionally aligned with fine cooling $\gamma'$-precipitates present within $\gamma$ channels (Figure 1(d2)). The fine $\gamma'$-precipitates were observed for all heat-treatments studied. For the final aging time of 1000 hours, the $\gamma'$-precipitates display a directionally coarsened microstructure.

The areal fraction of the primary $\gamma'$-precipitates was calculated from representative cross sections of the alloy by pixel-counting image analysis. The areal fraction following 50 and 100 hours of aging was ~50 pct, and decreases to 35 and 25 pct following 200 and 1000 hours of aging, respectively. It appears that this alloy has not achieved its equilibrium volume fraction at 1173 K (900 °C), after a 1000 hours temperature hold. It has been noted by Hadjiapostolidou and Shollock,[34] and Footner and Richards[35] that dissolution of $\gamma'$-precipitates in Ni superalloys occurs over long time periods at temperatures approaching the solvus temperature. In the present case, the holding temperature of 1173 K (900 °C) was 90 K (90 °C) below the solvus as determined by calorimetry.[19,20] Recently, Lass et al. studied the stability of ternary Co-Al-W alloys between 1023 K and 1373 K (750 °C and 1100 °C) in detail.[36] In their work, they suggest that the apparent stability of the ternary alloys at 1223 K (950 °C) is a consequence of slow kinetics of $\gamma'$ dissolution at this temperature, and the rate of dissolution increases if the hold temperature is lowered toward
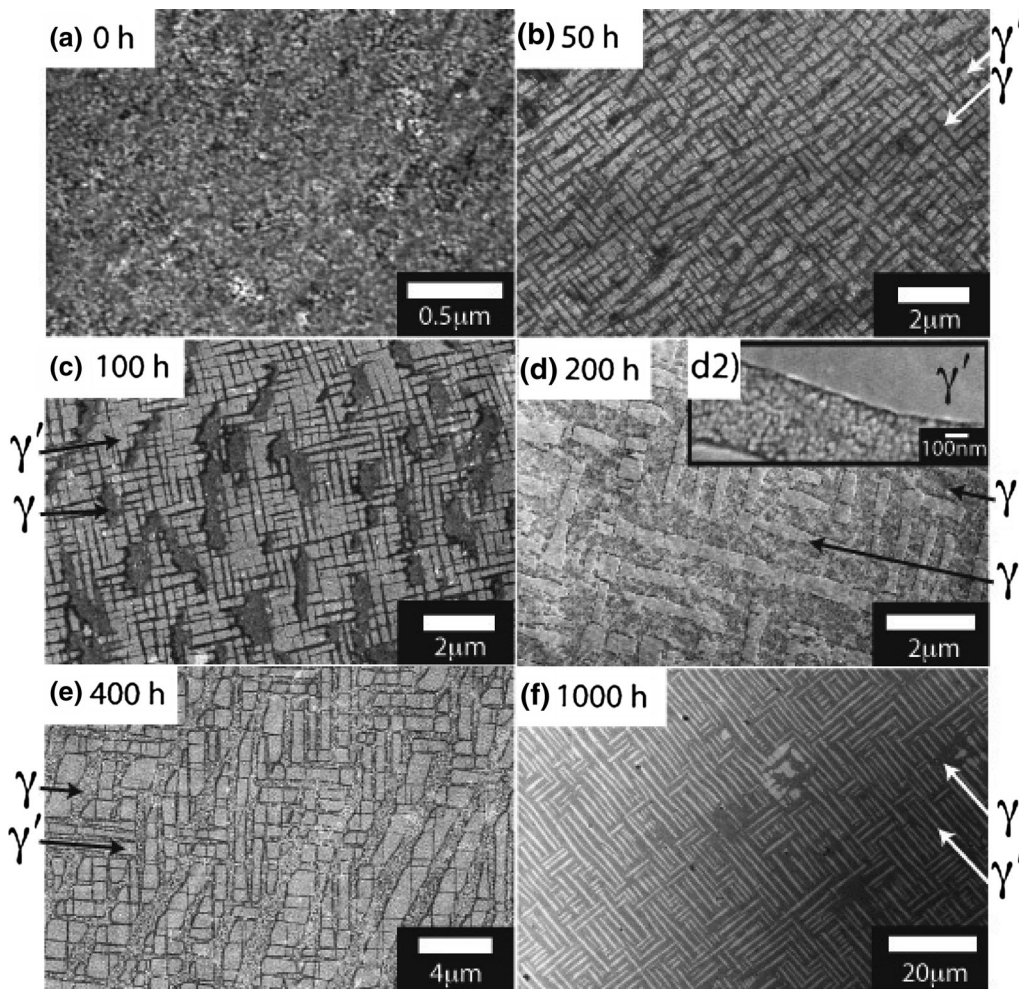
Fig. 1—Representative secondary emission SEM images of etched cross sections showing the evolution of the $\gamma'$-precipitates at 1173 K (900 °C) at time intervals of (a) 0 h, (b) 50 h, (c) 100 h, (d) 200 h, (e) 400 h, and (f) 1000 h. The magnification is progressively decreased with aging time, as the particles grow in size. Inset (d2) shows the fine $\gamma'$-precipitates that are present in the $\gamma$ channels for all aging conditions.

1123 K (850 °C). A time–temperature–transformation diagram constructed from their results shows a classic nose-shape indicative of the tradeoff between kinetics and thermodynamics.[36] Thus, referring to the study of the ternary Co-Al-W system by Lass et al.,[36] it is clear that the W-free superalloy in this work has not achieved phase stability nor its $\gamma'$ equilibrium volume fraction at 1173 K (900 °C).

Following the 1173 K (900 °C)/50 hours age, the precipitates are to a first approximation cuboidal. The mean width ($\bar{w}$) of the $\gamma'$-precipitates for this aging time was calculated from traced areas using square-equivalence ($\bar{w} = \overline{\text{area}}^{1/2}$) and found to be $\bar{w} = 220 \pm 70$ nm with standard deviation. Following the 1173 K (900 °C)/1000 hours age, the average width (determined by manually measuring 30 precipitates from traced areas) of the particles increases to $600 \pm 130$ nm, and the particle length (in the direction of coalescence) increases to $1400 \pm 110$ nm. In this case of decreasing volume fraction during aging, it is not physically reasonable to compare the particle growth rate to diffusion-controlled coarsening models. These models assume the amount of solute in the system ($C^0$) is conserved during coarsening,

that the matrix supersaturation decreases from its initial value to zero, and that the volume fraction ($V_f$) is a time-independent constant, thus conservation of mass is applied and given by $C^0 = (1 - V_f)C_\infty(t) + V_f C^\beta$, where $C_\infty(t)$ is the mean field concentration in the matrix and $C^\beta$ is the concentration of the precipitate phase.[37]

B. Microhardness Testing

The microhardness for different aging times at 1173 K (900 °C) ranges from 2.3 to 2.65 GPa, (Figure 2). The microhardness is initially 2.65 GPa and then decreases by 9 pct to 2.45 GPa after 1000 hours. During that time, the volume fraction of primary $\gamma'$-precipitates has decreased from 50 to 25 pct. Given that secondary $\gamma'$-precipitates are present following the cooling after each aging-treatment, this lack of change in hardness value may indicate that the secondary $\gamma'$-precipitates are controlling the room temperature microhardness independent of the contribution of the $\gamma'$-primary precipitates.[38,39] These $\gamma'$-precipitates will not, however, be present at elevated temperatures where the evolution of strength is anticipated to be different. An alternative

explanation is that the coarsened $\gamma'$-precipitates hinder dislocation motion more strongly than non-coalesced precipitates,[40,41] which compensates for the loss of strength due to the decrease in the primary $\gamma'$ volume fraction. Hot tensile or hot microhardness tests may shed light on this hypothesis.

## C. Creep

Grain size surface analysis was performed by optical analysis on a 900 °C/200 hours sample with $6 \text{ mm} \times 7 \text{ mm}$ surface area etched with Carappela's reagent. The grains were too large to establish an average grain size with reasonable counting statistics, but the mean grain width appears to be within 1 to 5 mm.

The first and second creep specimens, which were aged at 1173 K (900 °C) for 200 hours, were crept under compression at 1123 K (850 °C) for 97 and 664 hours, respectively. The specimens fractured after 8.3 and 7.0 pct strain, respectively. Cracks observed along the lateral and transverse planes following fracture are strongly indicative of intergranular failure. Bauer et al. previously noted that decohesion of the grain boundaries resulted in failure at early stages of creep of Co-Al-W-based alloys.[21]

Their minimum creep rate is plotted as a function of stress in Figure 3. The first creep specimen exhibits systematically higher minimum creep rates than the second one, with creep exponents n for both tests (n = 7.9 and 6.5), which are probably within error, given the limited number of data points. A data point for the ternary Co-Al-W alloy aged at 1173 K (900 °C)[21] is also plotted in Figure 3 for comparison. The creep performance of the lower density W-free superalloy is comparable to the ternary alloy.

Cross sections of the two specimens post-creep reveal directional coarsening of the $\gamma'$ phase perpendicular to the compressive load direction, Figures 4(a) and (c). This is consistent with a positive lattice parameter misfit between $\gamma'$-precipitates and $\gamma$-matrix. The misfit of all Co superalloys reported to date have been positive in value,

for example.[42] The first specimen shows directional coarsening after 97 hours of creep.

The width of precipitates taken parallel to applied load (longitudinal section) is $300 \pm 80$ nm for the first creep specimen, which is smaller than that of the second creep specimen which was crept for a much longer time, $630 \pm 170$ nm, Figures 4(b) and (d). The volume fraction of the first and second creep tests are within error (64 and 66 pct, respectively). These volume fractions are similar to the Co-9Al-9W at. pct crept sample investigated by Bauer et al. ($V_f \sim 60$ pct), that exhibited similar creep strength.[21] Owing to the larger precipitate size and greater extent of rafting of $\gamma'$-precipitates resulting from the longer creep time, we expect that dislocation creep is slower in the second specimen, which accounts for its higher creep strength.

In comparison with the previously described investigation of thermally induced particle evolution, it is noteworthy that the volume fraction of $\gamma'$ precipitates decreased significantly during a thermal hold of 1173 K (900 °C) over 1000 hours, while the volume fraction of $\gamma'$ has increased following the creep test at 1123 K (850 °C). As previously mentioned, the decrease in volume fraction at 1173 K (900 °C) thermal exposure, followed by a quench, is indicative of early onset of $\gamma'$ dissolution at a near $\gamma'$ solvus temperature,[34–36] where the work of Lass et al. indicates the Co-Al-W ternary $\gamma + \gamma'$ microstructure is not stable. This work indicates that the same may be true of Co-Al-Mo-Nb-based superalloys. At the lower creep temperature of 1123 K (850 °C), this onset of $\gamma'$ dissolution has not occurred in the creep tests lasting 97 hours and 664 hours. Again, this can be interpreted in light of the time-temperature-transformation diagram presented by Lass et al.,[36] where the onset of $\gamma'$ dissolution can occur at longer times as temperature is decreased. In the case of the 1123 K (850 °C) creep tests, the volume fraction appears to increase, perhaps indicating a small temperature region where the $\gamma'$ is in equilibrium; however, this appears to be unlikely.[36] Presumably, the lower temperature hold during creep, followed by furnace cooling within the creep rig, has precipitated further $\gamma'$, thereby increasing $\gamma'$ volume fraction. If the Co-Al-Mo-Nb system is similar to the Co-Al-W system, one would expect the onset of $\gamma'$ dissolution to occur at longer temperature holds at 1123 K (850 °C).[36] However, further future work is required on Co-Al-Mo-Nb $\gamma'$ stability to reach this conclusion.

The diagonal $\gamma$ channels across the $\gamma'$ rafts suggest shearing of the $\gamma'$ precipitates by extended antiphase boundaries,[13,25,26] Figure 4. Detailed studies of the dislocation-precipitate shear mechanisms, stacking faults, and antiphase boundaries formed during creep of CoNi-base superalloys are presented elsewhere under similar creep conditions but with tensile load.[13,25,26] The first sample also exhibited $\gamma$ channels cutting the $\gamma'$ rafts; however, it was far more extensive in the second sample, presumably, a consequence of the higher creep stresses applied to the alloy and the longer time-length creep test. Eggeler et al.[25] concluded that $\gamma'$ shearing events are more frequent at greater creep strains.
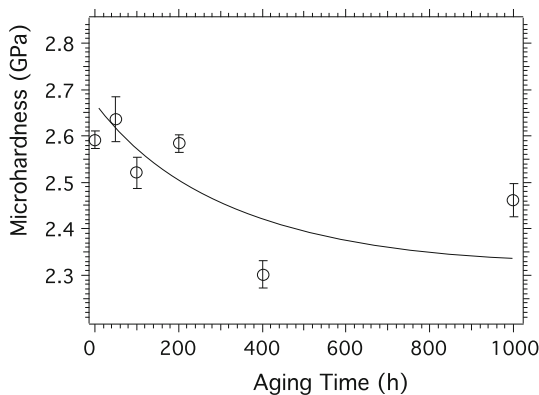


Fig. 2—Evolution of room-temperature microhardness as a function of aging time for aging times between 0 and 1000 h at 1173 K (900 °C). A trend line has been added as an aid to the eye.

## D. Neutron Diffraction

Figure 5 displays the time-of-flight neutron diffraction spectrum of Co-30Ni-9.9Al-5.1Mo-1.9Nb at. pct alloy at room temperature and zero load condition, after aging at 1073 K (800 °C) for 200 hours. $\gamma'$ is an ordered $L1_2$ superlattice, therefore $\{hkl\}$ all odd/all even (e.g., $\{200\}$, $\{111\}$) peaks are composites of $\gamma + \gamma'$ due to scattering from both phases, whereas the other $\{hkl\}$ peaks (e.g., $\{110\}$, $\{210\}$) arise only from the $L1_2$ $\gamma'$ phase, Figure 5. Measurements were made of the $\{111\}$,

$\{200\}$, $\{220\}$, $\{222\}$, $\{400\}$, and lower d-space composite reflections. The $\{110\}$ is the only superlattice reflection that was distinguishable from background. A pseudo-Voigt profile was fitted to the $\{110\}$ and $\{220\}$ peaks using Wavemetrics Igor software. Small lattice mismatch and large intrinsic widths prevent direct deconvolution of the superlattice reflections. The $\{220\}$ composite doublet peak was fitted using a routine,[29–31,42] assuming (i) equal instrumental peak widths of $\gamma$ and $\gamma'$, (ii) equal Voigt shape function of both $\gamma$ and $\gamma'$, (iii) the $\{220\}$ $\gamma'$ position is fixed from the $\gamma'$ $\{110\}$, and (iv) the intensity ratios of each phase comprising the $\{220\}$ doublet was defined from the approximate volume fraction of $\gamma'$ ($V_f \sim 0.5$), giving $I_\gamma : I_{\gamma'}$ 1 : 1. The final fitting parameters were the overall intensity, width, shape function, and location of the $\gamma$-peak. The composite fit is shown in the inset of Figure 5. The $\{110\}$ $\gamma'$ d-space is found to be $2.5361 \pm 0.0013$ Å, yielding a lattice parameter $a_{\gamma'} = 3.587 \pm 0.001$ Å from Bragg's law for a cubic system. Constraining the $\{220\}$ $\gamma'$ position from the $\{110\}$ reflection and using the doublet fitting routine described previously, the $\{220\}$ $\gamma$ position is found to be $1.2641 \pm 8.43 \times 10^{-05}$ Å; the real error in the $\{110\}$ $\gamma$ peak position must be greater than or equal to the error of the $\{220\}$ $\gamma'$ position. The lattice parameter of $\gamma$ is therefore $a_\gamma = 3.575 \pm 0.001$ Å. Using these lattice parameter values to calculate misfit $\delta = 2(a_{\gamma'} - a_\gamma)/(a_{\gamma'} + a_\gamma)$, gives a positive misfit of $+0.32 \pm 0.15$ pct, if one assumes a 5 pct error in the methodology. This fit and misfit value is similar to that employed by Pyczak et al. for Co-10Al-8W at. pct measured by synchrotron XRD.[43] Their alloy possessed very similar lattice
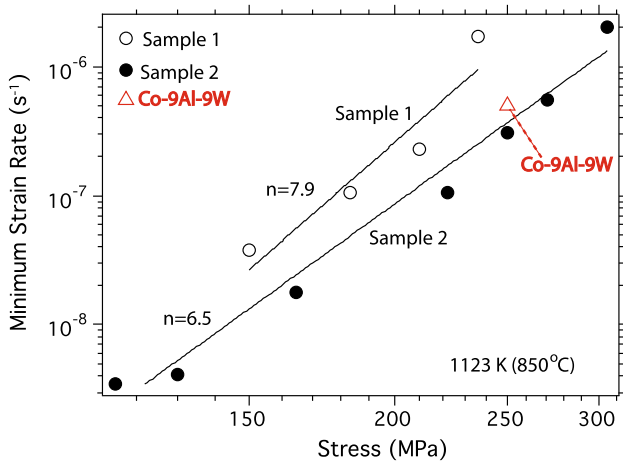


Fig. 3—Minimum creep strain rate *vs* engineering stress for Co-30Ni-9.9Al-5.1Mo-1.9Nb and Co-9Al-9W at. pct alloys[21] alloy tested at the same temperature, 1123 K (850 °C) . The W-free alloy performs comparably to the W-containing alloy.
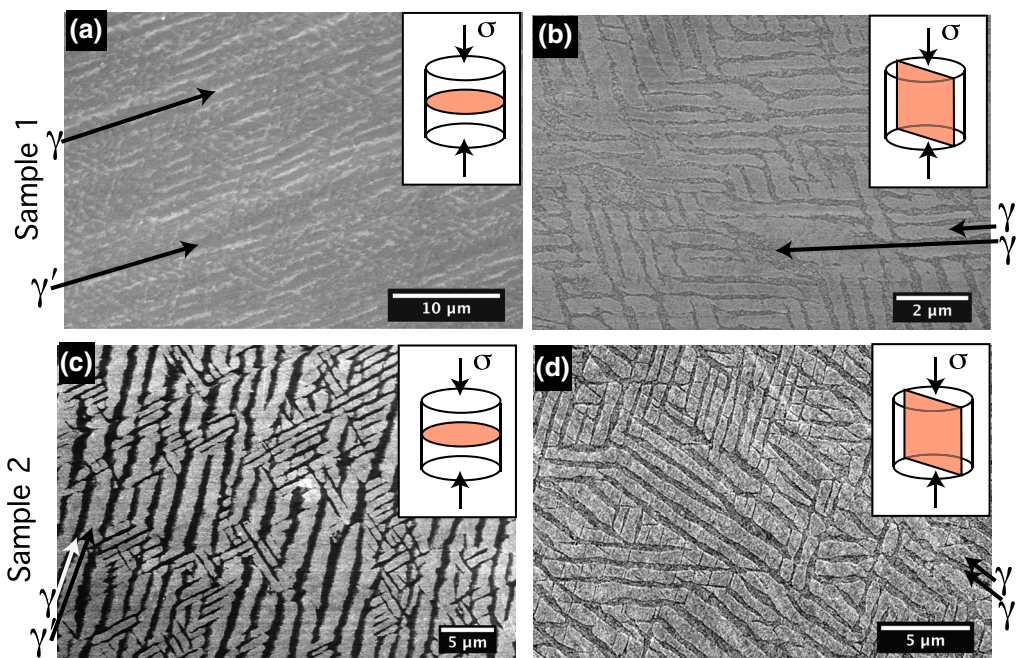


Fig. 4—Representative SEM images of etched cross sections displaying rafting of the $\gamma'$-precipitates as a result of compressive creep strain for creep specimens 1 and 2, tested at 1123 K (850 °C) for 97 and 664 h, respectively. Schematics have been added to show the surfaces imaged and stress directions. (a) Specimen 1 cut perpendicular to loading direction, and (b) parallel to the loading direction. (c) Specimen 2 cut perpendicular to loading direction, and (b) parallel to the loading direction. Figures (a) through (c) are secondary emission images, and (d) is backscatter.

parameters and misfit at room temperature: $a_{\gamma'} = 3.589$ Å; $a_\gamma = 3.576$ Å; and $\delta = 0.36$ pct. In their work, they showed that the misfit of Co-9Al-9W at. pct is essentially constant to a threshold temperature of $\sim 873$ K (600 °C), above which it decreases in magnitude. This may be due to the onset of dissolution of $\gamma'$-precipitates. Importantly, the misfit does not change the sign to negative values at any elevated temperature. Given the similarity in lattice parameters and misfit of the alloy studied in this work to those studied by Pyczak *et al.*, it is reasonable to assume that Co-30Ni-9.9Al-5.1Mo-1.9Nb at. pct maintains a positive misfit value at elevated temperatures.

## IV. SUMMARY AND CONCLUSIONS

In summary, a Co-30Ni-9.9Al-5.1Mo-1.9Nb at. pct superalloy is aged at 1173 K (900 °C) to develop a coherent $\gamma/\gamma'$ microstructure. The $\gamma'$-precipitates morphology, volume fraction, and dimensions are investigated for aging up to 1000 hours. The precipitate morphology evolves from a cuboidal microstructure after aging for 50 hours, to a directionally coarsened microstructure of elongated aligned rectangular cuboid shapes, observed after aging for 200 hours. The primary precipitate volume fraction decreases from 50 to 25 pct after aging for 1000 hours at 1173 K (900 °C), thus the alloy has not reached its equilibrium stable state at this temperature. The particle length increases from $\sim 220$ to $\sim 1400$ nm between 50 and 1000 hours of aging.

This evolution to a directionally coarsened microstructure with decreased volume fraction leads to a modest decrease in the room-temperature microhardness, from 2.65 to 2.45 GPa, possibly because they are strengthened by secondary $\gamma'$-precipitates created during cooling. Alternatively, the larger coalesced $\gamma'$-precipitates may be superior to the non-coalesced precipitates in hindering dislocation motion and strengthening the alloy, which compensates for the loss of strength due to the decrease in volume fraction. The creep strength of the W-free cobalt alloy at 1123 K (850 °C), after aging at 1173 K (900 °C) for 200 hours, is comparable to that of the basic W-containing Co-9Al-9W at. pct superalloy. The post-creep microstructure of the W-free alloy shows that rafting is occurring perpendicular to the applied stress, in agreement with a positive lattice parameter misfit between the $\gamma$- and $\gamma'$-phases as measured by neutron diffraction.

Fig. 5—Neutron diffraction spectrum for Co-30Ni-9.9Al-5.1Mo-1.9Nb at. pct polycrystal superalloy aged at 1073 K (800 °C) for 200 h. The (110) is a $\gamma'$-reflection, while the other reflections are composite peaks of $\gamma + \gamma'$ phases. Inset: (220) composite peak fit, the (220) $\gamma'$ position was constrained by the location of the (110) reflection.

## REFERENCES

1. R.C. Reed: *The Superallloys: Fundamentals and Applications*, Cambridge University Press, Cambridge, 2006.
2. C.T. Sims, N.S. Stoloff, and W.C. Hagel: *Superalloys II: High-Temperature Materials for Aerospace and Industrial Power*, Wiley, New York, 1987.
3. T.M. Pollock and S. Tin: *J. Propuls. Power*, 2006, vol. 22, pp. 361–74.
4. E. Nembach and G. Neite: *Prog. Mater. Sci*, 1985, vol. 29, pp. 177–19.
5. P. Caron: *Superalloys, 9th International Symposium on Superalloys*, TMS, 2000, pp. 737–46.
6. V. Deodeshmukh, N. Mu, B. Li, and B. Gleeson: *Surf. Coat. Technol.*, 2006, vol. 201, pp. 3836–40.
7. A.M. Khan, S. Sundarrajan, S. Nataragan, P. Parameswaran, and E. Mohandas: *Mater. Manuf. Process.*, 2014, vol. 29 (7), pp. 832–39.
8. J. Sato, T. Omori, K. Oikawa, I. Ohnuma, R. Kainuma, and K. Ishida: *Science*, 2006, vol. 312, pp. 90–91.
9. F. Xue, H.J. Zhou, M.L. Wang, X.F. Ding, and Q. Feng: *Mater. Lett.*, 2013, vol. 112, pp. 215–18.
10. K. Shinagawa, T. Omori, K. Oikawa, R. Kainuma, and K. Ishida: *Scripta Mater.*, 2009, vol. 61, pp. 612–15.
11. M. Titus, A. Suzuki, and T.M. Pollock: *Scripta Mater.*, 2012, vol. 66, pp. 574–77.
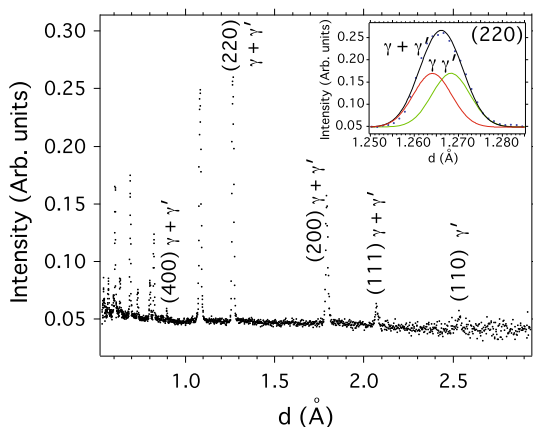12. K. Tanaka, M. Ooshima, N. Tsuno, A. Sato, and H. Inui: *Phil. Mag.*, 2012, vol. 92, pp. 4011–27.

13. M.S. Titus, Y.M. Eggeler, A. Suzuki, and T.M. Pollock: *Acta Mater.*, 2015, vol. 82, pp. 530–39.
14. H.Y. Yan, V.A. Vorontsov, J. Coakley, N.G. Jones, H.J. Stone, and D. Dye: *Superalloys, 12th International Symposium on Superalloys*, TMS, 2012, pp. 705–14.
15. L. Klein, M.S. Killian, and S. Virtanen: *Corros. Sci.*, 2013, vol. 69, pp. 43–49.
16. M. Knop, P. Mulvey, F. Ismail, A. Radecka, K.M. Rahman, T.C. Lindley, B.A. Shollock, M.C. Hardy, M.P. Moody, T.L. Martin, P.A.J. Bagot, and D. Dye: *JOM*, 2014, vol. 66, pp. 2495–2501.
17. S. Neumeier, H.U. Rehman, J. Neuner, C.H. Zenk, S. Michel, S. Schuwalow, J. Rogal, R. Drautz, and M. Göken: *Acta Mater.*, 2016, vol. 106, pp. 304–12.
18. A. Suzuki, H. Inui, and T.M. Pollock: *Annu. Rev. Mater. Res.*, 2015, vol. 45, pp. 345–68.
19. S.K. Makineni, B. Nithin, and K. Chattopadhyay: *Scr. Mater.*, 2015, vol. 98, pp. 36–39.
20. S.K. Makineni, B. Nithin, and K. Chattopadhyay: *Acta Mater.*, 2015, vol. 85, pp. 85–94.
21. A. Bauer, S. Neumeier, F. Pyczak, R.F. Singer, and M. Göken: *Mater. Sci. Eng. A*, 2012, vol. 550, pp. 333–41.
22. A. Bauer, S. Neumeier, F. Pyczak, and M. Göken: *Superalloys 2012: 12th International Symposium on Superalloys*, 2012, pp. 695–703.
23. F. Xue, H.J. Zhou, Q.Y. Shi, X.H. Chen, H. Chang, M.L. Wang, and Q. Feng: *Scr. Mater.*, 2015, vol. 97, pp. 37–40.
24. F. Xue, H.J. Zhou, and Q. Feng: *JOM*, 2014, vol. 66 (12), pp. 2486–94.
25. Y.M. Eggeler, M.S. Titus, A. Suzuki, and T.M. Pollock: *Acta Mater.*, 2014, vol. 77, pp. 352–59.
26. Y.M. Eggeler, J. Müller, M.S. Titus, A. Suzuki, T.M. Pollock, and E. Spiecker: *Acta Mater.*, 2016, vol. 113, pp. 335–49.
27. F.R.N. Nabarro: *Metall. Mater. Trans. A*, 1996, vol. 27A, pp. 513–30.
28. H. Mughrabi: *Acta Mater.*, 2014, vol. 81, pp. 21–29.
29. D. Dye, J. Coakley, V.A. Vorontsov, H.J. Stone, and R.B. Rogge: *Scripta Mater.*, 2009, vol. 61, pp. 109–12.
30. J. Coakley and D. Dye: *Scripta Mater.*, 2012, vol. 67, pp. 435–38.
31. J. Coakley, R.C. Reed, J.L.W. Warwick, K.M. Rahman, and D. Dye: *Acta Mater.*, 2012, vol. 60, pp. 2729–38.
32. F.J. Radd and L.H. Crowder: *Nature*, 1958, vol. 181, pp. 258–59.
33. K. An: *ORNL Report*, 2012, ORNL-TM-2012-621, pp.1–19.
34. D. Hadjiapostolidou and B.A. Shollock: *Superalloys, 11th International Symposium on Superalloys*, TMS, 2008, pp. 733–39.
35. P.K. Footner and B.P. Richards: *J. Mater. Sci.*, 1983, vol. 18, pp. 1896–97.
36. E.A. Lass, R.D. Grist, and M.E. Williams: *J. Phase. Equilib. Diffus.*, 2016, vol. 37 (4), pp. 387–401.
37. J. Coakley, H. Basoalto, and D. Dye: *Acta Mater.*, 2010, vol. 58, pp. 4019–28.
38. K. Kakehi: *Mater. Sci. Eng A.*, 2000, vol. 278 (1–2), pp. 135–41.
39. D. Locq, P. Caron, S. Raujol, F. Pettinari-Sturmel, A. Coujou, and N. Clément: *Superalloys, 10th International Symposium on Superalloys*, TMS, 2004, pp. 179–87.
40. P. Caron and T. Khan: *Mater. Sci. Eng.*, 1983, vol. 61 (2), pp. 173–84.
41. U. Tetzlaff and H. Mughrabi: *Superalloys, 9th International Symposium on Superalloys*, TMS, 2000, pp. 273–82.
42. H.Y. Yan, J. Coakley, V.A. Vorontsov, N.G. Jones, H.J. Stone, and D. Dye: *Mater. Sci. Eng. A*, 2014, vol. 613, pp. 201–08.
43. F. Pyczak, A. Bauer, M. Göken, U. Lorenz, S. Neumeier, M. Oehring, J. Paul, N. Schell, A. Schreyer, A. Stark, and F. Symanzik: *J. Alloys Compd.*, 2015, vol. 632, pp. 110–15.